

Particle Image Velocimetry Measurements of Rigid and Flexible Rectangular Wings Undergoing Main Flapping Motion in Hovering Flight

Srikanth Goli, Arnab Roy, Devendra Kumar Patel
and Subhransu Roy

Abstract The present work is focused on flow field behavior generated by rigid and flexible rectangular wings undergoing main flapping motion using two dimensional Particle Image Velocimetry (PIV). The experiments have been carried for an asymmetry one degree of freedom main flapping motion of both rigid and flexible low aspect ratio wings at 1 Hz flapping frequency in hovering flight mode (advanced ratio, $J = 0$) at zero geometric angle of attack, zero wing pitch angle and chord wise based Reynolds number of the order of 10^4 along the wings spanwise direction at its mid chord to obtain instantaneous flow fields. The improved understanding of effect of wake capture, observation of spanwise flow on the wing, and formation-growth-diffusion of wingtip vortices have been achieved. Effect of wing flexibility on the flow field has been studied by comparing the flow field of both rigid and flexible rectangular wings undergoing main flapping motion.

Keywords Particle Image Velocimetry · Flapping motion · Hovering flight · Flapping wing · Micro air vehicle

1 Introduction

Micro air vehicles (MAV) have various applications in military and civilian purposes like collection of biological/chemical samples from hazardous zone and explosive detection in public places, border security etc. and in monitoring traffic, wildlife, pipeline and real estate aerial photography, are much useful for public

Srikanth Goli · Arnab Roy (✉)

Department of Aerospace Engineering, Indian Institute of Technology, Kharagpur, India
e-mail: arnab@aero.iitkgp.ernet.in

D.K. Patel · Subhransu Roy

Department of Mechanical Engineering, Indian Institute of Technology, Kharagpur, India

© Springer India 2017

A.K. Saha et al. (eds.), *Fluid Mechanics and Fluid*

Power – Contemporary Research, Lecture Notes in Mechanical Engineering,

DOI 10.1007/978-81-322-2743-4_135

safety in fire and rescue operations by smoke and sound detection. In order to fulfill the requirements of extremely challenging applications of MAV's, the flying vehicles should be small, should possess hover capability, perching capability, and high maneuverability. These qualities can be achieved by flapping flight; the best example could be the natural flyers. Earlier works Hong and Altman [1] carried out PIV measurements for flapping wings in air at flapping frequencies in the order of 3–6 Hz. Jardin et al. [2] carried experiments for a pitching NACA0012 profile rigid wings at flapping frequency 10 Hz and Re no. in the order of 10^3 . Suryadi et al. [3] focused on flapping rigid plate and Jones and Babinsky [4] worked on waving rigid wings. Lua et al. [5] studied on linearly moving 2D rigid wings. Ozen and Rockwell [6] carried out PIV measurements for rigid wings in forward flight at Re no. of the order of 10^3 .

The present study is focused on achieving an improved understanding of certain aspects of flapping wing aerodynamics like the effect of wake capture, observation of spanwise flow on the wing, and formation-growth-diffusion of wingtip vortices. Effect of wing flexibility on the flow field has been studied by comparing the flow field of both rigid and flexible rectangular wings undergoing main flapping motion. In the present study, 1:3 ratios lower half stroke to upper half stroke asymmetry one degree of freedom main flapping motion of both rigid and flexible low aspect ratio wings at 1 Hz flapping frequency have been investigated in hovering flight mode (advanced ratio, $J = 0$) at zero geometric angle of attack, zero wing pitch angle and chord wise based Reynolds number of the order of 10^4 using phase-locked 2D PIV measurements along the wings spanwise direction at its mid chord to obtain instantaneous flow fields.

2 Experimental Setup

2.1 Main Flapping Mechanism and Water Tank

The flapping mechanism has been built in the Department of Aerospace Engineering at Indian Institute of Technology Kharagpur. The design of the mechanism is similar to that reported in Mazaheri and Ebrahimi [7] (Patent lies with Kim et al. [8] “Cybrid P1 remotely controlled ornithopter”). The four bar mechanism as shown in Fig. 1, in which the DC motor is connected to the pinion, transform the rotational motion to desired main flapping motion. The driving motor is powered directly by a stable DC power supply, by which the flapping frequency is controlled by altering the input voltage. The experiments have been carried out in a water tank with dimensions of $304.8 \times 304.8 \times 304.8 \text{ mm}^3$ volume as shown in Fig. 2.

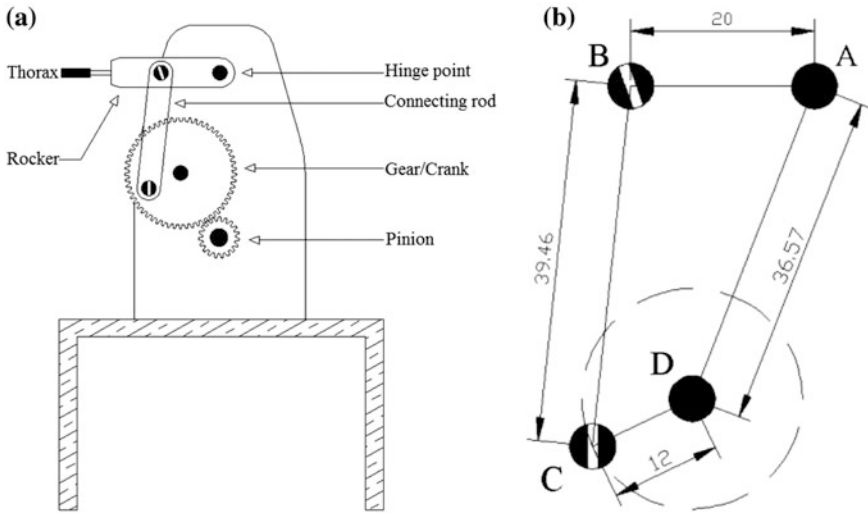


Fig. 1 Schematic of a Main flapping mechanism and b Mechanical linkage (dimensions in mm)

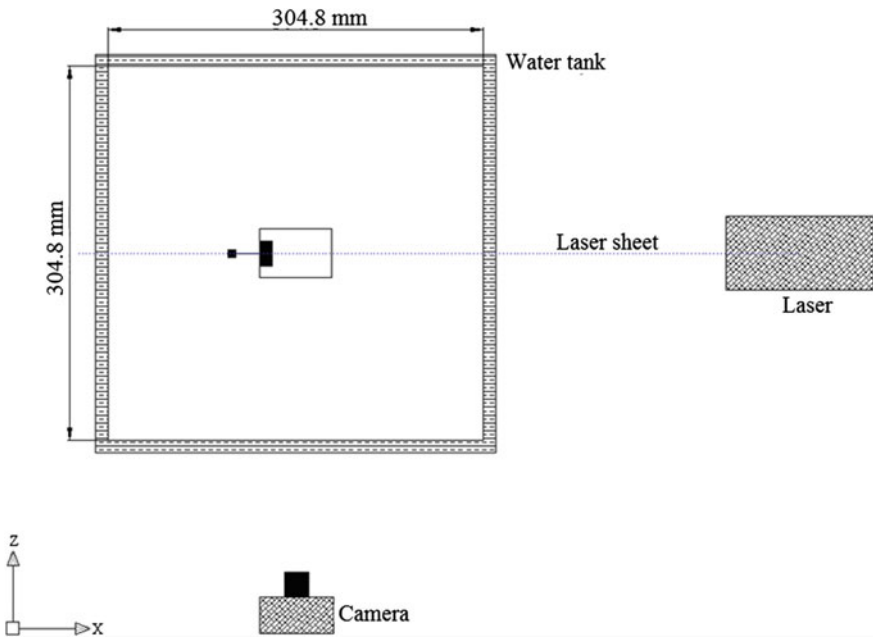


Fig. 2 Schematic plan view of setup and wing position (along the spanwise direction)

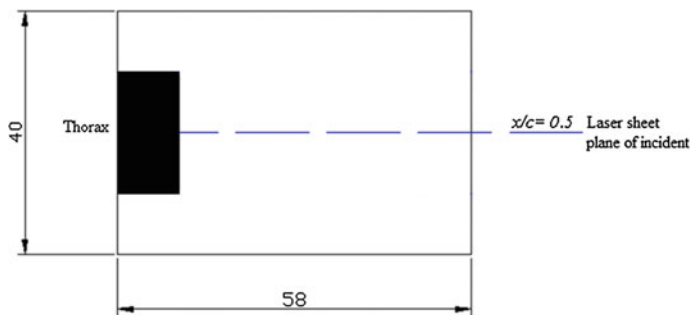


Fig. 3 Plan view of rectangular wing (dimensions in mm)

2.2 Wing Details

The dimensions of the wings as shown in Fig. 3 and Table 1. The dimensions of thorax were length of 20 mm, width of 10 mm and thickness of 3 mm with 2 grams in weight.

2.3 Experimental Procedure

The flapping mechanism is mounted on a test stand and fully immersed in the water tank with free top surface with the fluid initially maintained in quiescent condition (hover). The experiments have been performed with the nominal flapping amplitude of 80° (ϕ), with upper half stroke angle (ϕ_a) of 60° and lower half stroke angle (ϕ_b) of 20° from the horizontal line, with zero wing pitch angle and at flapping frequency of 1 Hz. During the experiments, the actual achieved flapping amplitude (ϕ) with wings attached to the main flapping mechanism is different from nominal flapping amplitude due to inertial loads as shown in Table 2. The flapping amplitude depends on the parameters like wing shape, wing area, wing materials and operating conditions.

Table 1 Wing parameters

Wing planform type	Material	Aspect ratio, AR	Thickness (mm)	Weight (gms)	Planform area, A (mm ²)
Rectangular	Rigid (PVC)	1.45	1.5	4	2320
Rectangular	Flexible (PE)	1.45	0.26	<0.5	2320

Table 2 Achieved flapping amplitude

Wing type	ϕ (°)	ϕ_a (°)	ϕ_b (°)
Rectangular wing (rigid)	70.65	53.45	17.2
Rectangular wing (flexible)	78.06	58.15	19.91

The flow parameters like Reynolds number is obtained of 1.14×10^4 and 1.26×10^4 for rigid wing and flexible wing respectively and reduced frequency is 1.59 for rigid wing and 1.76 for flexible wing.

PIV measurements have been performed for both rigid and flexible rectangular wing after 300 strokes of flapping cycles for the flow to achieve periodic state of unsteadiness. The tests have been conducted along the mid span of the wing, where the laser sheet was aligned to the mid chord of the wing. The analysis has been carried out for 150 flapping strokes which include 75 downstrokes and 75 upstrokes.

2.4 PIV System and Data Processing

The PIV system consist Nd: YAG Laser with maximum energy/pulse 150 mJ, wave length 1064 nm, Laser pulse rate of 14.5 Hz, and the CCD camera equipped with a 1600×1200 pixel resolution, 32 fps has been used. TSI INSIGHT 3GTM software is used to process the captured images by a cross correlation technique with interrogation window size maintained at 24×24 pixels, 25 % overlapping with a time delay of 250 μ s between two frames. The water is seeded by Nylon particles with a mean diameter of 4 μ m, density of 1.14 g/cc. The percentage of seeding particles is approximately 10^{-4} (24 ml water laden with particles mixed with 28,000 ml of clean water).

3 Results and Discussion

3.1 Rigid Rectangular Wing

The Figs. 4 and 5 show the instantaneous velocity vector field for a rigid rectangular wing during downstroke and upstroke of the flapping cycle respectively. At the beginning of the downstroke ($\phi = 52.22^\circ$) a wing tip vortex called primary TV1 has

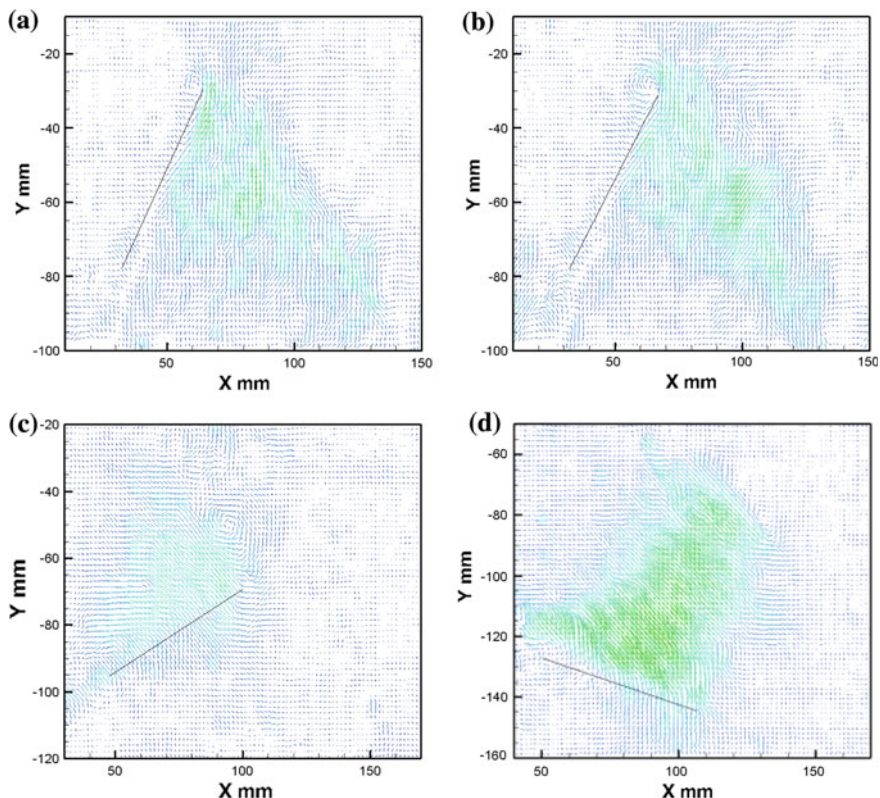


Fig. 4 Instantaneous velocity vector fields for a rigid rectangular wing during downstroke of flapping cycle. **a** $\phi = 52.22^\circ$. **b** $\phi = 51.50^\circ$. **c** $\phi = 24.16^\circ$. **d** $\phi = -17.20^\circ$

been formed above the wing (inboard direction), due to the spanwise flow below the wing generated by previous strokes. Then onwards TV1 grows in size ($\phi = 51.5^\circ$) and at $\phi = 49.06^\circ$ TV1 gets detached from the wing, and not much spanwise flow is observed. TV1 has been diffused into the wake at $\phi = 40.18^\circ$. At $\phi = 24.16^\circ$, secondary TV2 has been formed by gaining strength from previous shed vorticity as the wing accelerates. Then again a new secondary TV forms and sheds in the wake. This process has been continuously observed till the end of downstroke. Spanwise flow increases as the wing reaches the end of the downstroke. In a similar manner, at the beginning of the upstroke ($\phi = -16.52^\circ$) a primary TV1 forms below the wing, it then grows in size and gets detached from the wing at $\phi = -13.35^\circ$. As the

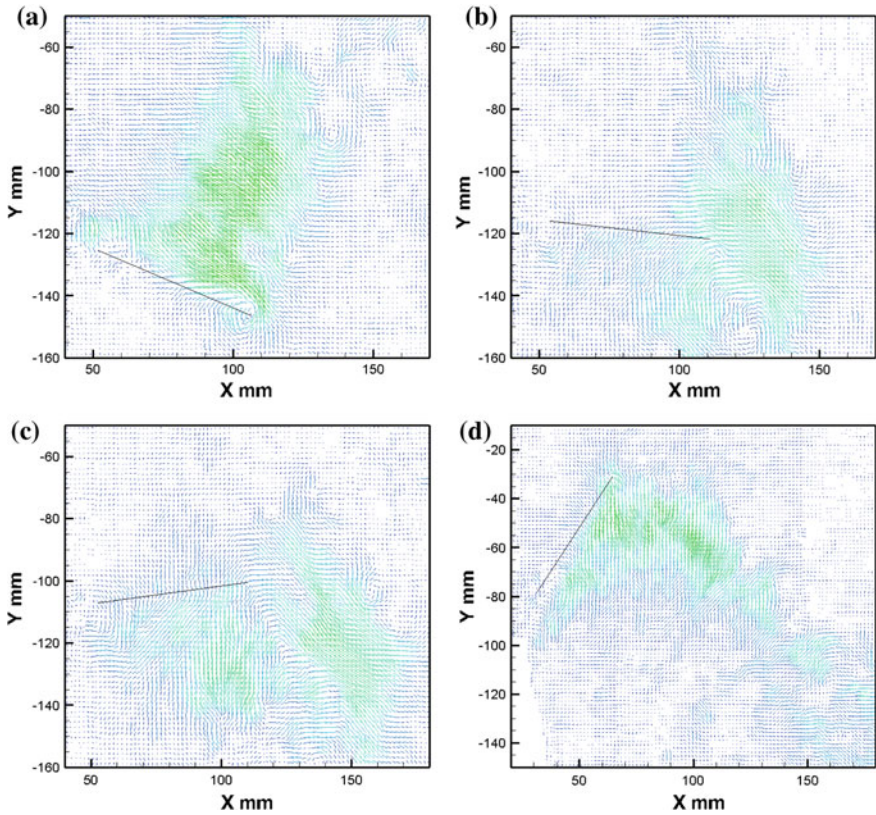


Fig. 5 Instantaneous velocity vector fields for a rigid rectangular wing during upstroke of flapping cycle. **a** $\phi = -16.52^\circ$. **b** $\phi = -04.92^\circ$. **c** $\phi = 07.17^\circ$. **d** $\phi = 53.45^\circ$

wing accelerates toward the end of the upstroke a spanwise flow is observed, however, no secondary TV is observed as during the downstroke.

3.2 Flexible Rectangular Wing

The Figs. 6 and 7 show the instantaneous velocity vector field for a flexible rectangular wing during downstroke and upstroke of the flapping cycle respectively. At the beginning of the downstroke ($\phi = 51.1^\circ$) a pair of counter rotating vortices have been formed at wingtip with a substantial spanwise flow below the wing. At $\phi = 46.15^\circ$ the vortex in the inboard direction gets stronger than the outboard vortex. Then the vortex pair detaches from the wing ($\phi = 41.39^\circ$) while they keep growing in size. From then a substantial spanwise flow above the wing has been

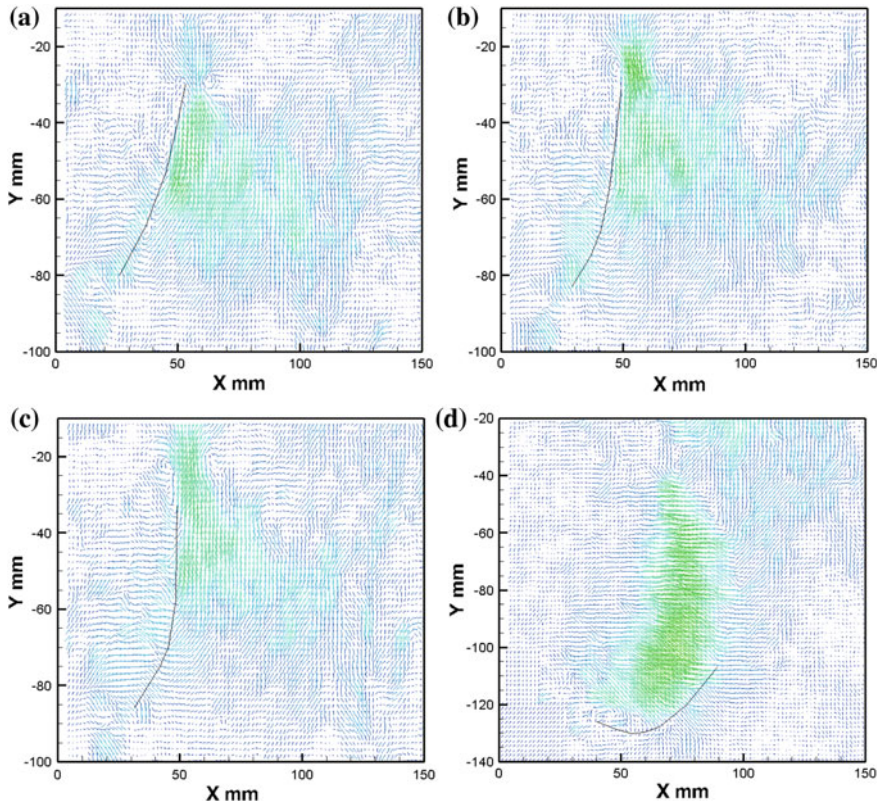


Fig. 6 Instantaneous velocity vector fields for a flexible rectangular wing during downstroke of flapping cycle. **a** $\phi = 51.10^\circ$. **b** $\phi = 46.15^\circ$. **c** $\phi = 41.39^\circ$. **d** $\phi = -19.91^\circ$

observed and continuous formation and shedding of secondary TV2 is observed throughout the downstroke.

At the beginning of the upstroke ($\phi = -9.75^\circ$) a pair of vortices- one above and other below the wing along with spanwise flow above the wing has been observed. At $\phi = -0.55^\circ$ the pair vortex grows in size and detach from the wing. At $\phi = 14.08^\circ$ the pair vortex moves far away from the wing and secondary vortex TV2 above the wing has been observed due to previous strokes. At $\phi = 21.35^\circ$ pair vortex and secondary vortex diffuses into the wake and slight spanwise flow begins below the wing. From $\phi = 35.85^\circ$ to end of the upstroke ($\phi = 58.15^\circ$), no spanwise vortices have been observed while the fluid follows the wing underneath.

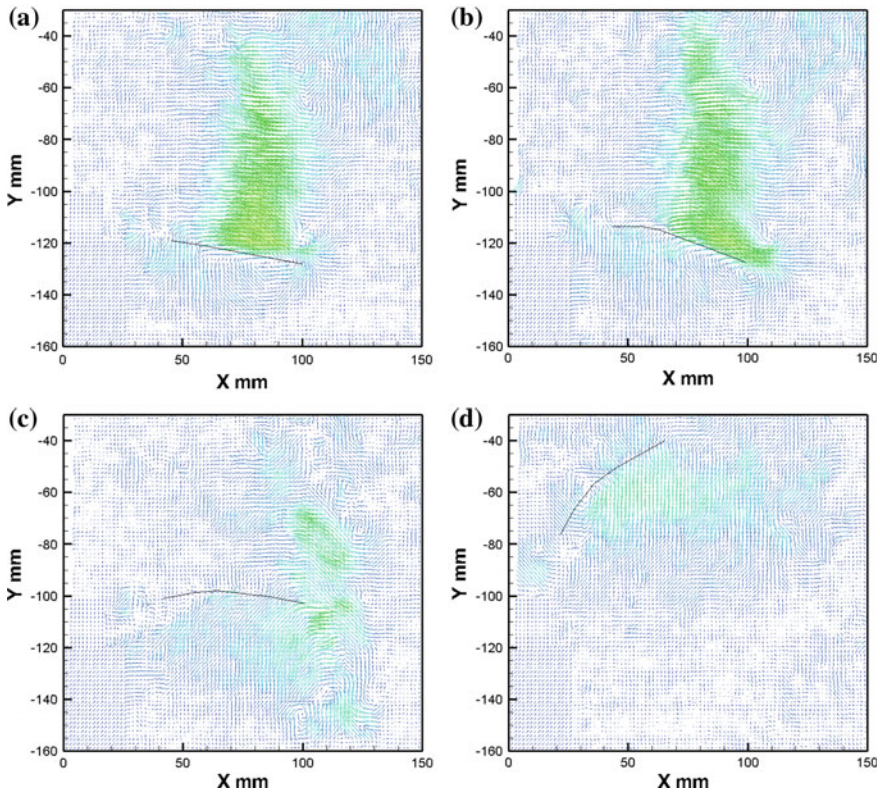


Fig. 7 Instantaneous velocity vector fields for a flexible rectangular wing during upstroke of flapping cycle. **a** $\phi = -9.75^\circ$. **b** $\phi = -0.55^\circ$. **c** $\phi = 14.08^\circ$. **d** $\phi = 58.15^\circ$

4 Conclusions

1. In the rigid rectangular wing, at the beginning of each stroke, a wing tip vortex (TV) forms in the inboard direction due to spanwise flow generated by previous strokes. This is likely to result in upwash and downwash associated with positive and negative lift forces at the wingtip.
2. In the case of rigid rectangular wing, the spanwise flow due to wake capture is weaker than flexible rectangular wing. This is likely to result in achieving positive and negative lift forces at early part of each stroke w.r.t downstroke and upstroke.
3. In the case of flexible rectangular wing, at the beginning of each stroke, pair of vortices is formed due to spanwise flow generated by previous strokes and possibly due to LEV detachment and subsequent interaction with TV. This is

due to chordwise wing deformation and also because at the beginning of each stroke, wing-root & wing-tip moves in opposite direction.

4. In the case of flexible rectangular wing, the flow is dominated by strong downward and upward advection induced by the wing causing higher flapping amplitude than the other case. This is likely to result in delayed positive and negative lift forces w.r.t downstroke and upstroke.

References

1. Hong, Y.S., Altman, A.: Lift from spanwise Flow in simple flapping wings. *J. Aircr.* **45**, 1206–1216 (2008)
2. Jardin, T., David, L., Farcy, A.: Characterization of vortical structures and loads based on time-resolved PIV for asymmetric hovering flapping flight. *Exp. Fluids* **46**, 847–857 (2009)
3. Suryadi, A., Ishii, T., Obi, S.: Stereo PIV measurements of a finite, flapping rigid plate in hovering condition. *Exp. Fluids* **49**, 447–460 (2010)
4. Jones, A.R., Babinsky, H.: Unsteady lift generation on rotating wings at low Reynolds Numbers. *J. Aircr.* **47**, 1013–1021 (2010)
5. Lua, K.B., Lim, T.T., Yeo, K.S.: Effect of Wing-Wake Interaction on Aerodynamic Force Generation on a 2D Flapping Wing
6. Ozen, C.A., Rockwell, D.: Vortical structures on a flapping wing. *Exp. Fluids* **50**, 23–34 (2011)
7. Mazaheri, K., Ebrahimi, A.: Experimental investigation of the effect of chordwise flexibility on the aerodynamics of flapping wings in hovering flight. *J. Fluids Struct.* **26**, 544–558 (2010)
8. Kim, S.W., Jang, L.H., Kim, M.H., Kim, J.S.: Power-driven ornithopter piloted by remote controller, Patent No: US 6,550,716 B1 (2003)